Evidence for the Three-Center Elimination of HCl from CH_3CHClO

M. Matti Maricq,* Jichun Shi,† Joseph J. Szente, L. Rimai, and E. W. Kaiser*

Research Laboratory, Ford Motor Company, P.O. Box 2053, Drop 3083/SRL, Dearborn, Michigan 48121

*Received: June 4, 1993; In Final Form: July 22, 1993**

Time-resolved IR spectral photography and transient diode laser absorption measurements reveal a yield of HCl from the photolysis of Cl_2 in the presence of C_2H_5Cl and O_2 which is 78% larger than expected from Cl + C_2H_5Cl. The HCl formation occurs in two steps: a rapid rise to [HCl] = $[Cl]_0$, followed by a secondary rise to [HCl] = $1.78[Cl]_0$ with a rate constant of $k_3 = (5.2 \pm 1.3) \times 10^{-12}$ cm^3 s^{-1}. In the presence of NO, the rate of secondary HCl formation is greatly enhanced, but its yield (84%) is comparable to that in the absence of NO. The secondary HCl is explained as an elimination product from the CH_3CHClO, which can be generated by the reaction of CH_3CHClO_2 with itself or with NO. The fact that the secondary HCl yield increases by 12% when using CD_3CH_2Cl shows that the secondary HCl is formed mainly by three-center elimination from the 1-chloroethoxy radical. We also report UV absorption cross sections for CH_3CHClO_2, which has a broad maximum of $\sigma_{max} = 0.029$ Å^2 from 215 to 248 nm, and $CH_2ClCH_2O_2$, with $\sigma_{max} = 0.045$ Å^2 at 240 nm. The self-reaction rate constants are $(5.2 \pm 1.3) \times 10^{-12}$ cm^3 s^{-1} and $(6.0 \pm 0.8) \times 10^{-12}$ cm^3 s^{-1}, respectively. Finally, the rate constant for the reaction Cl + C_2H_5Cl = C_2H_4Cl + HCl (1) is determined to be $k_1 = (7.3 \pm 0.9) \times 10^{-12}$ cm^{-3} s^{-1}.

I. Introduction

Of considerable interest to the atmospheric oxidation of hydrocarbons and the accompanying photochemical smog formation is the fate of organic alkoxy radicals. These species are formed in the atmosphere in the following manner. Hydrocarbons from biogenic or anthropogenic sources, which are emitted into the atmosphere, are attacked by OH radicals (also NO_3, and in the laboratory Cl or F). These abstract a hydrogen atom producing an alkyl radical which then rapidly adds molecular oxygen to form a peroxy (RO_2) radical. These species will subsequently react with NO or another organic peroxy radical to form the corresponding alkoxy radical.[1] The alkoxy radical, in general, has three fates in the atmosphere.[2] The predominant fate is reaction with O_2 to form an aldehyde or ketone and HO_2, with the latter product going on to regenerate the OH radical. Decomposition and isomerization are usually minor pathways. However, counterexamples include CF_3CFHO which primarily dissociates into CF_3 and HCOF at O_2 pressures below about 500 Torr,[3,4] and the related alkoxy radicals,[5,6] CF_3CF_2O and CF_2HCF_2O, which follow analogous decomposition pathways.

Recently, evidence for a new decomposition pathway has been discovered in which HCl is eliminated from CH_3CHClO. The results of a FTIR product study of the Cl-initiated oxidation of ethyl chloride have been presented in a previous paper.[7] This study revealed the formation of significantly higher levels of HCl than can be accounted for by the primary reaction between Cl and C_2H_5Cl in conjunction with a high yield of CO_2 (≈50%). Neither observation is consistent with the known alkoxy radical degradation pathways;[2] thus, a mechanism involving HCl elimination from CH_3CHClO was postulated in ref 7. The present paper reports direct, time-dependent measurements of the HCl and CH_3CHClO_2 concentrations which are used to help establish the chemical reaction mechanism.

Although HCl elimination from the chloroethoxy radical is unusual, there have been a number of studies of HCl and HF elimination from substituted alkanes.[8-12] A topic of current debate is the question of whether reactions of the form H + RF$^\bullet$ → R + HF or Cl + R$^\bullet$ → R′ + HCl proceed by direct abstraction or via addition/elimination. Seakins et al.[8,9] and Arunan et al.[10] have measured the nascent vibrational distributions of the HCl and HF produced in these reactions and interpret these results as supporting the addition/elimination mechanism. On the other hand, the kinetic data of Tsai and McFadden[11] suggest that direct abstraction may be important. What differentiates these systems from the HCl elimination by CH_3CHClO, however, is their energetics. The previous studies involve elimination from intermediates with on the order of 100 kJ/mol excess energy above the reaction barrier.[8,10] The generation of the alkoxy radical via

$$CH_3CHClO_2 + CH_3CHClO_2 \rightarrow 2CH_3CHClO + O_2 \quad (3a)$$

however, is likely to be nearly thermoneutral; the analogous reactions for methyl and ethyl peroxy radicals have exothermicities of $\Delta H = 0$ an 16 kJ/mol, respectively.[13] That the resultant alkoxy radical eliminates HCl is, thus, quite intriguing.

In this paper, the mechanism of the secondary HCl production is examined by time-resolved spectroscopic techniques. UV absorption is used to monitor the parent CH_3CHClO_2 radicals while HCl formation is probed by IR spectroscopy. The experimental techniques are reviewed in section II, and the IR and UV measurements are discussed in sections III and IV, respectively.

II. Experimental Section

(a) TRISP. The time-resolved IR spectroscopy (TRISP) apparatus and technique have been described in detail.[14,15] Visible radiation near 430 nm from a broad-band, pulsed dye laser is used to generate pulsed, broad-band infrared (IR) radiation (2700–3200 cm^{-1}) by stimulated electronic raman scattering (SERS) in a rubidium vapor heat pipe. The IR probes a reacting mixture flowing through a cylindrical (1.7 cm i.d. × 6 cm long) five-pass cell with BaF_2 windows in which a photochemical reaction has been initiated by pulsed laser radiation. The consumption of reactants and generation of products can thus be observed on time scales as short as the laser pulse width (<20 ns). After passing through the cell, the IR is shifted into the visible-wavelength range by four-wave mixing in a second rubidium heat pipe, synchronously pumped by a narrow-band, pulsed dye laser, to facilitate detection of the IR spectrum. The visible radiation, which contains the IR signature, is dispersed by a monochromator

† Current address: Procter and Gamble Co., 5299 Spring Grove Ave. Room A-100E, Cincinnati, OH 45217-1087.

* Abstract published in *Advance ACS Abstracts*, September 1, 1993.

0022-3654/93/2097-9686$04.00/0

and imaged on a silicon-intensified target vidicon controlled by an optical multichannel analyzer.

A reacting mixture containing Cl_2, C_2H_5Cl, and air flows through the cell at a total rate of 14 L/min, which provides complete cell purging between the photolysis pulses of a XeF excimer laser at 351 nm. The reactant flow rates were calibrated by measuring the rate of pressure rise in a known volume. In addition, samples of the flowing reactant mixture were withdrawn downstream of the reactor for gas chromatographic (GC) analysis to verify the ethyl chloride concentration. The total pressure in the reactor is maintained at 760 Torr.

The pulsed 351-nm radiation (250 mJ at the cell), which photolyzes the molecular chlorine, is focused onto the side of the reactor in a band that overlaps as uniformly as possible the axially directed IR probe radiation. The IR probe pulse reaches the reaction cell at a predetermined variable delay time (350 ns to 1 ms) following the onset of the photolysis reaction to measure the HCl concentration as a function of reaction time. The HCl was quantified by measuring the absorbance of the IR radiation by the $m = -1$, -2, -3, and -4 lines of the P branch.

(b) Transient IR Absorption. A detailed description of the flash photolysis, transient infrared absorption apparatus has been given previously.[12] Briefly, a ≈300-mJ pulse of 351-nm radiation from a Lambda Physik LPX-300 excimer laser is directed longitudinally through a 3.2-cm diameter by 51-cm-long fused silica reaction cell and is used to dissociate molecular chlorine in a $Cl_2/C_2H_5Cl/O_2/N_2$ gas mixture. Except for the determination of k_1, the concentrations of ethyl chloride (2.8 Torr) and oxygen (50 Torr) are chosen sufficiently large that the reactions

$$Cl + C_2H_5Cl \rightarrow C_2H_4Cl + HCl \quad (1)$$

$$C_2H_4Cl + O_2 + M \rightarrow C_2H_4ClO_2 + M \quad (2)$$

occur on a time scale of a microsecond. For the measurement of k_1 the C_2H_5Cl level was decreased to 0.76 Torr.

Infrared radiation from a Pb salt diode laser (Laser Analytics) counterpropagates the reaction vessel via dichroic optics which reflect at 351 nm but transmit IR light and probes the volume swept out by the photolysis laser beam. A single mode of the diode laser is selected by a monochromator, which also removes scattered light and fluorescence due to the excimer laser pulse. The IR light is detected by a HgCdTe detector with a 200-ns response time, and the resultant signal is digitized by a Data Precision 6000 transient recorder. The diode laser is frequency locked to the R(2) line of $H^{35}Cl$ ($H^{37}Cl$), which at 100 Torr of N_2 has an absorption cross section of 0.135 ± 0.011 Å² (0.046 ± 0.002 Å²) (errors are 95% confidence intervals as determined from the scatter of seven independent measurements). For many of the results reported below, however, the effect of the error in HCl cross section is eliminated, or at least significantly reduced, by measuring the transient absorbance arising from the HCl formed by photolysis of a $C_2H_5Cl/Cl_2/O_2/N_2$ gas mixture relative to the absorbance due to the HCl produced in a $C_2H_6/Cl_2/O_2/N_2$ gas mixture under identical experimental conditions.

The transient change in IR light intensity following the flash photolysis is converted into a change in HCl concentration using Beer's law:

$$c(t) = -\ln[(I_b + I(t))/I_0]/\sigma_{IR}l$$

with l representing the path length and σ_{IR} the HCl IR cross section. Because the HgCdTe detector is ac coupled, the constant component of the IR light intensity, I_b, is added to the transient signal prior to ratioing it with I_0. The ac coupling also causes the detector response to decay with a rate constant of $k_{det} = 600$ s^{-1} following a step function change in light intensity. This decay is slow in comparison to the rise in [HCl]. It is taken into account in the modeling by augmenting the kinetic equations with

$$\frac{dV}{dt} = \frac{d}{dt} e^{-[HCl]_t \sigma_{IR} l} - k_{det} V$$

where $V(t)$ represents the output voltage of the IR detector, and then applying Beer's law to the result in order to extract the predicted HCl concentration dependence in the presence of the detector decay.

Ordinarily, one must consider the possibility that HCl is born vibrationally excited. In the present case, however, this is unnecessary for the following reasons. The exothermicity of primary HCl formation via Cl + C_2H_5Cl is sufficiently small (7.5 kcal[16]) to allow at most a minor amount of vibrational excitation of the product HCl. While the thermodynamics of the HCl elimination from CH_3CHClO is unknown, it is unlikely for this process to have enough exothermicity to produce highly excited HCl molecules. Even if formed, vibrationally excited HCl would be rapidly, if incompletely, relaxed at the 100–760-Torr conditions under which the experiments were carried out.[17] HCl, in ground or excited states, from other sources, such as the radical–radical reaction between Cl and C_2H_4Cl, is insignificant because of the large (20–150 Torr) amounts of O_2 employed. Finally, excited HCl would go undetected by the present IR measurements, implying that the measured HCl concentrations represent lower limits. However, these lower limits account stoichiometrically for the HCl expected from the proposed reaction mechanism.

(c) Time-Resolved UV Spectral Photography. The apparatus for monitoring CH_3CHClO_2 radicals by their UV absorption[18] is essentially the same as was described in section IIb for the transient IR measurements. The main differences are that the diode laser is replaced by a deuterium lamp and the HgCdTe detector is replaced by a gated, intensified, diode array detector (Princeton Instruments IPDA-700SB detector and ST1000 controller). Also, the optics are changed to allow transmission of 190–330-nm light while reflecting the 351-nm excimer radiation. The UV spectra are calibrated against the output of a low-pressure Hg lamp and have a resolution of approximately 3 nm.

The time resolved absorbances are converted into concentrations by a least-squares fit to the reference UV spectra of the relevant species; thus

$$Abs(t,\lambda) = \sigma_a(\lambda)\, l c_a(t) + \sigma_b(\lambda)\, l c_b(t) + \ldots$$

where l is the path length and $\sigma_i(\lambda)$ and $c_i(t)$ are, respectively, the absorption cross section and the concentration of species i. The initial chlorine atom concentration is obtained by substituting C_2H_6 for C_2H_5Cl in the flowing gas mixture and recording the ethylperoxy absorbance 20 μs following laser photolysis. The absorbance is then converted into concentration using the known $C_2H_5O_2$ UV absorption cross section[18] and equating this with $[Cl]_0$.

Gas flows were controlled by Tylan flow controllers, except for the chlorine flow which was set by a needle valve. Relative flows were determined by measuring the rate of pressure rise of each component in a constant volume and the partial pressures calculated from the fractional flow and the total pressure. C_2H_6 and C_2H_5Cl were obtained from Matheson and O_2 and N_2 from Airco and were used without further purification.

III. IR Measurements

The principal conclusions presented in this paper are based on the unexpected time dependence observed for the evolution of HCl following the Cl initiated oxidation of ethyl chloride. This is illustrated in Figure 1 by a plot of HCl concentration versus time, determined by the TRISP apparatus. The evolution is characterized by a rapid ($t_{1/2} < 500$ ns) initial rise of HCl to a level equal to $[Cl]_0$, followed by a much slower ($t_{1/2} \approx 10$ μs) secondary rate of HCl formation. As we demonstrate in the

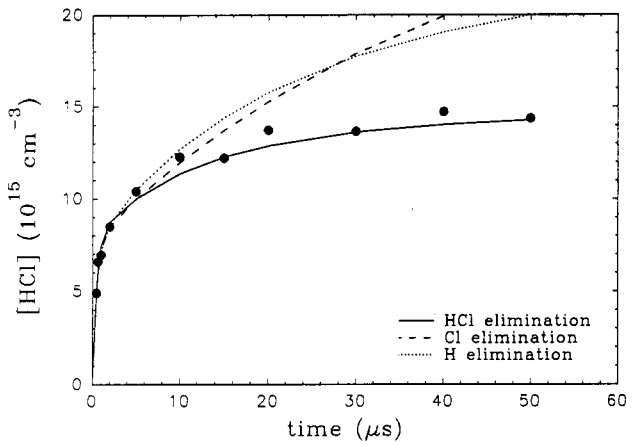

Figure 1. TRISP data showing the HCl concentration vs time after the photolysis of a Cl_2 (34 Torr)/C_2H_5Cl (9.8)/O_2 (150)/N_2 (566) gas mixture. The solid line is the fit to the data with $[Cl]_0 = 8.1 \times 10^{15}$ cm^{-3} using the mechanism in Table I (see section IIIb). Dashed line, substitute reaction 25 for reaction 6. Dotted line, substituted reaction 26 for reaction 6.

ensuing discussion, this peculiar time dependence originates because of three-center HCl elimination from the CH_3CHClO radical.

(a) Primary HCl Formation. The reaction mechanism used to model the HCl and CH_3CHClO_2 kinetic measurements reported below is presented in Table I (by far the principal reactions needed to model the HCl formation, in excess O_2, are reaction 1, 2, 3, and 6). Within this model, the primary generation of HCl occurs from Cl atom attack on ethyl chloride, reactions 1a and 1b.

The diode laser measurements of HCl formation were performed in pairs; one experiment employed ethyl chloride and the second ethane. If we temporarily ignore complications from the secondary HCl generation, then for both the ethane and ethyl chloride mixtures the HCl concentration should vary as $[HCl](t) = [Cl]_0(1 - \exp(-k[RH]t))$ to zeroth order. This implies that the ratio $[HCl]_{etcl}/[HCl]_{et}$ does not depend on $[Cl]_0$. Furthermore, the HCl IR absorption cross section is not needed to determine the concentration ratio from the ratio of absorbances. Thus, fitting the experimentally measured $[HCl]_{etcl}/[HCl]_{et}$ ratio to model predictions eliminates the effects of possible systematic errors in $[Cl]_0$, σ_{IR}, and the detector decay on the determination of k_1. Note that this is not a relative rate measurement in the conventional sense, because the HCl generated by either ethyl chloride or ethane is measured in separate experiments and not in a competitive reaction between chlorine and these two reactants. Nonetheless, knowledge of the rate constant k_A (=Cl + C_2H_6) is required to evaluate k_1. Because $k_A \approx 7k_1$,[19] a 10% error in k_A will produce only a 1.5% error in the determination of k_1, and very accurate measurements of k_1 are, therefore, possible using this technique.

In practice, there is a small effect of the secondary HCl on the primary HCl formation rate. This is taken into account by fitting the ratio between the HCl predicted from the reaction model of Table I and that predicted from C_2H_6 (which essentially appears in a step function) to the experimental HCl ratio. The results from two experiments at different C_2H_5Cl concentrations are $k_1 = (7.5 \pm 0.6) \times 10^{-12}$ cm^3 s^{-1} and $(6.8 \pm 1.1) \times 10^{-12}$ cm^3 s^{-1} for 0.76 and 3.8 Torr of C_2H_5Cl, respectively. The dashed line in Figure 2A illustrates the fit between the experimental [HCl] ratio and the ratio derived from the model for the 0.76-Torr initial C_2H_5Cl concentration. The errors in the rate constant (95% confidence intervals) are a statistical combination of the fitting error and a 5% error due to uncertainties in the C_2H_5Cl concentration.

There is a possible problem with the analysis of the primary

TABLE I: Reaction Mechanism

no.	reaction	rate constant at 295 K
1a	$Cl + C_2H_5Cl \rightarrow CH_3CHCl + HCl$	$k_{1a} = 6.0 \times 10^{-12}$ cm^3 s^{-1} [a]
1b	$Cl + C_2H_5Cl \rightarrow CH_2ClCH_2 + HCl$	$k_{1b} = 1.2 \times 10^{-12}$ cm^3 s^{-1} [a]
2a	$CH_3CHCl + O_2 + M \rightarrow CH_3CHClO_2 + M$	$k_{2a} = 5 \times 10^{-12}$ cm^3 s^{-1} [b]
2b	$CH_2ClCH_2 + O_2 + M \rightarrow CH_2ClCH_2O_2 + M$	$k_{2b} = 5 \times 10^{-12}$ cm^3 s^{-1} [b]
3a	$CH_3CHClO_2 + CH_3CHClO_2 \rightarrow 2CH_3CHClO + O_2$	$k_{3a} = (4.9 \pm 1.2) \times 10^{-12}$ cm^3 s^{-1} [a]
3b	$CH_3CHClO_2 + CH_3CHClO_2 \rightarrow CH_3CClO + CH_3CHClOH + O_2$	$k_{3b} = (0.3 \pm 0.3) \times 10^{-12}$ cm^3 s^{-1} [a]
4	$CH_3CHClO_2 + CH_2ClCH_2O_2 \rightarrow CH_3CHClO + CH_2ClCH_2O + O_2$	$k_4 = 5.2 \times 10^{-12}$ cm^3 s^{-1}
5	$CH_2ClCH_2O_2 + CH_2ClCH_2O_2 \rightarrow 2CH_2ClCH_2O + O_2$	$k_5 = 6.0 \times 10^{-12}$ cm^3 s^{-1} [a]
6	$CH_3CHClO \rightarrow CH_3CO + HCl$	$k_{6a} > 5 \times 10^5$ s^{-1} [a]
7	$CH_3CO + O_2 + M \rightarrow CH_3C(O)O_2 + M$	$k_7 = 2 \times 10^{-12}$ cm^3 s^{-1} [20]
8a	$CH_3CHClO_2 + CH_3C(O)O_2 \rightarrow CH_3CHClO + CH_3CO_2 + O_2$	$k_{8a} = 1.5 \times 10^{-11}$ cm^3 s^{-1} [c]
8b	$CH_2ClCH_2O_2 + CH_3C(O)O_2 \rightarrow CH_2ClCH_2O + CH_3CO_2 + O_2$	$k_{8b} = 1.5 \times 10^{-11}$ cm^3 s^{-1} [c]
9	$CH_3C(O)O_2 + CH_3C(O)O_2 \rightarrow 2CH_3CO_2 + O_2$	$k_9 = 1.7 \times 10^{-11}$ cm^3 s^{-1} [21]
10	$CH_3CO_2 \rightarrow CH_3 + CO_2$	$k_{10} = 10^6$ s^{-1} [d]
11	$CH_3 + O_2 + M \rightarrow CH_3O_2 + M$	$k_{11} = 3.8 \times 10^{-13}$ cm^3 s^{-1} [22]
12a	$CH_3CHClO_2 + CH_3O_2 \rightarrow CH_3CHClO + CH_3O + O_2$	$k_{12a} = 2 \times 10^{-12}$ cm^3 s^{-1} [c]
12b	$CH_2ClCH_2O_2 + CH_3O_2 \rightarrow CH_2ClCH_2O + CH_3O + O_2$	$k_{12b} = 2 \times 10^{-12}$ cm^3 s^{-1} [c]
13a	$CH_3C(O)O_2 + CH_3O_2 \rightarrow CH_3CO_2 + CH_3O + O_2$	$k_{13a} = 1.2 \times 10^{-11}$ cm^3 s^{-1} [23]
13b	$CH_3C(O)O_2 + CH_3O_2 \rightarrow CH_3C(O)OH + HCHO + O_2$	$k_{13b} = 2.0 \times 10^{-12}$ cm^3 s^{-1} [23]
14a	$CH_3O_2 + CH_3O_2 \rightarrow 2CH_3O + O_2$	$k_{14a} = 1.2 \times 10^{-13}$ cm^3 s^{-1} [24]
14b	$CH_3O_2 + CH_3O_2 \rightarrow CH_2O + CH_3OH + O_2$	$k_{14b} = 2.8 \times 10^{-13}$ cm^3 s^{-1} [24]
15	$CH_3O + O_2 \rightarrow HO_2 + CH_2O$	$k_{15} = 1.3 \times 10^{-15}$ cm^3 s^{-1} [20]
16	$CH_2ClCH_2O + O_2 \rightarrow HO_2 + CH_2ClCHO$	$k_{16} = 8 \times 10^{-15}$ cm^3 s^{-1} [e]
17	$HO_2 + CH_3CHClO_2 \rightarrow CH_3CHClOOH + O_2$	$k_{17} = 7 \times 10^{-12}$ cm^3 s^{-1} [c]
18	$HO_2 + CH_3C(O)O_2 \rightarrow$ products	$k_{18} = 1.5 \times 10^{-11}$ cm^3 s^{-1} [23]
19	$HO_2 + CH_3O_2 \rightarrow$ products	$k_{19} = 5 \times 10^{-12}$ cm^3 s^{-1} [24]
20	$HO_2 + HO_2 \rightarrow$ products	$k_{20} = 3 \times 10^{-12}$ cm^3 s^{-1} [24]
21	$Cl + RO_2 \rightarrow ClO + RO$[g]	$k_{21} = 9 \times 10^{-12}$ cm^3 s^{-1} [25]
22	$ClO + RO_2 \rightarrow ClO_2 + RO$[g]	$k_{22} = 1 \times 10^{-11}$ cm^3 s^{-1} [25]
23	$Cl + O_2 + M = ClO_2 + M$[g]	$k_{23} = 1.4 \times 10^{-33}$ cm^6 s^{-1} [26]
24	$CH_3CHCl + Cl_2 \rightarrow CH_3CHCl_2 + Cl$[g]	$k_{24} = 2.2 \times 10^{-12}$ cm^3 s^{-1} [f]

[a] Measured in this work. [b] Taken as typical of alkyl + O_2 addition rate constants. See refs 20 and 22. [c] Assumed from closest analogous peroxy–peroxy reaction rate constant. See, e.g., refs 20, 22, and 24. [d] The value 2.2×10^{10} s^{-1} is reported in ref 21; however, increasing the rate to this value has no effect on the model predictions. [e] Assumed rate constant for ethoxy radical.[20] [f] Determined from ratio $k_{24}/k_{2a} = 0.42$.[14] [g] Reactions 21–24 were used to fit the TRISP data only (see text).

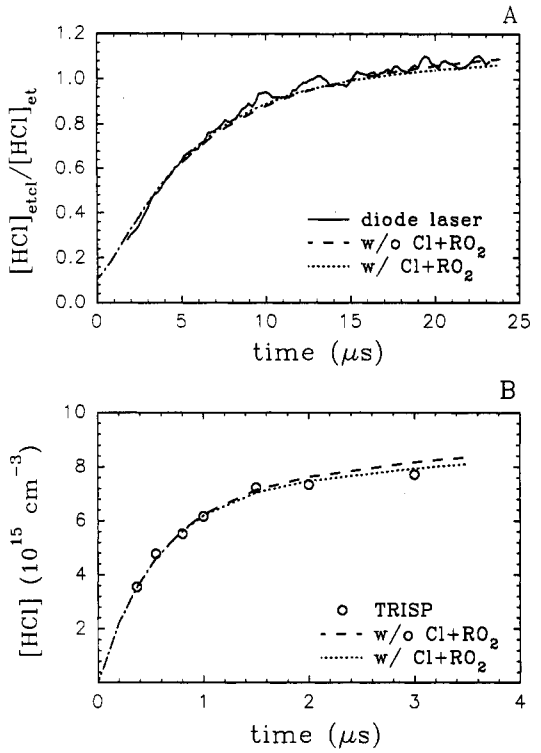

Figure 2. Comparison of experiment with model predictions for the primary HCl formation from the chlorine initiated oxidation of C_2H_5Cl. (A) Diode laser measurements with $[Cl]_0 = 9.1 \times 10^{14}$ cm^{-3} and $[C_2H_5Cl]_0 = 0.76$ Torr. (B) TRISP measurements with $[Cl]_0 = 7.3 \times 10^{15}$ cm^{-3}, $[C_2H_5Cl]_0 = 7.3$ Torr, $[Cl_2] = 20$ Torr, $[O_2] = 150$ Torr, $[N_2] = 568$ Torr, and $k_1 = 7.67 \times 10^{-12}$ cm^3 s^{-1}. The dotted and dashed lines show the effect of reaction 21 on the model predictions. Individual points are the experimental data.

HCl rise time based on the reaction model of Table I. Time-dependent UV absorption spectra show that increasing amounts of ClO are formed as the C_2H_5Cl concentration is reduced from about 3 to 0.1 Torr (with $[Cl]_0 \approx 10^{15}$ cm^{-3}).[25] We postulate that the ClO arises from the reaction

$$Cl + CH_3CHClO_2 \rightarrow ClO + CH_3CHClO \qquad (21)$$

which our preliminary data[25] show to occur with a rate constant of $\approx 9 \times 10^{-11}$ cm^3 s^{-1}. ClO generation with a fast rate constant ($>1 \times 10^{-10}$ cm^{-3} s^{-1}) has been observed for another Cl + peroxy radical reaction (Cl + CF_2ClO_2) by Dagaut et al.[27] Fortuitously, reaction 21 has little effect on the primary HCl generation in the diode laser experiments, because the CH_3CHClO radical rapidly dissociates via eq 6 and yields the HCl molecule that would have been produced had the chlorine atom reacted with C_2H_5Cl instead of the peroxy radical. The minimal effect is illustrated by the dotted line in Figure 2A, which shows the predicted HCl concentration when reaction 21 is added to model.

Figure 2B presents the HCl profile measured at reaction times less than 3 μs for one representative set of experimental conditions using the TRISP technique. Because of sensitivity limitations, the TRISP data are obtained using initial Cl atom concentrations 4–5 times larger than the maximum for the diode laser experiments. In addition, the fast response time of the TRISP technique allows measurements to be made at initial C_2H_5Cl concentrations up to 3 times larger than the maximum for the diode laser technique. Thus, results from the two techniques are obtained under very different experimental conditions and are complementary. For the TRISP data, values of $(Cl)_0$ and k_1 were determined for each experiment by fitting data such as presented in Figure 2B to the expanded mechanism in Table I. Reaction classes 21–23 were added for these fits because the higher radical concentrations of the TRISP experiments made them potentially more important. In addition, the chain propagating reaction 24

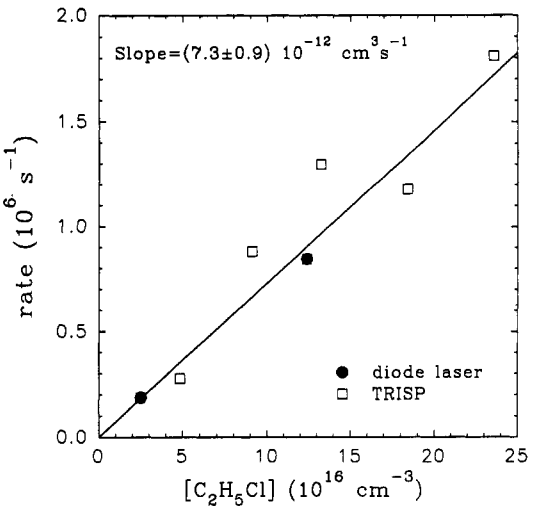

Figure 3. Cl + C_2H_5Cl reaction rate vs ethyl chloride concentration. Reactant concentrations for the TRISP data are similar to those in Figure 2.

was added because the Cl_2/O_2 ratio was approximately 15 times larger than for the diode laser experiments, leading to approximately 5% chain regeneration of Cl atoms. The preliminary rate constant for reaction 21 presented above was used for all possible Cl + RO_2 reactions in the mechanism. The UV data which identified ClO as a product of reaction 21 also showed a decay of ClO at longer times which was consistent with a ClO + RO_2 reaction with a rate constant in our system of $\approx 1 \times 10^{-11}$ cm^3 s^{-1}. This is similar to the value ($=(3 \pm 1.7) \times 10^{-12}$) derived for ClO + CH_3O_2 by Simon et al.[28] Reaction 22 and the decomposition of its assumed ClO_2 product via reaction 23 were also included in the mechanism used for the TRISP analyses. For the data at high C_2H_5Cl concentrations, these three reactions affect the determination of k_1 by <2% as shown by the dashed line in Figure 2B for which the rate of reaction 21 was set to zero. They can produce changes of ≈10% in the value of k_1 which is required to fit the data at the lowest initial C_2H_5Cl concentration. Thus, throughout the C_2H_5Cl concentration range, the effect of reactions 21–23 is of marginal significance. This expanded mechanism has been used in all TRISP analyses both for determination of k_1 and for modeling the secondary HCl generation in the following section.

The eight determinations of k_1 using both diode laser and TRISP have been plotted as a function of the ethyl chloride concentration in Figure 3. A fit to these data gives $k_1 = (7.3 \pm 0.9) \times 10^{-12}$ cm^3 s^{-1}, including statistical error plus 5% uncertainty in $[C_2H_5Cl]$. The value of k_1 reported here represents a refinement (improved signal to noise and a better reaction model) of the value $(6.8 \pm 1.4) \times 10^{-12}$ cm^3 s^{-1} previously reported from this laboratory by Kaiser et al.[14] using the TRISP technique. The new value agrees to well within the error limits with the absolute rate measurements by Wine and Semmes[29] which yielded a rate constant of $(8.04 \pm 0.54) \times 10^{-12}$ cm^3 s^{-1} at 297 K. It also shows satisfactory agreement with the relative rate measurement of $(8.7 \pm 1.0) \times 10^{-12}$ cm^3 s^{-1} by Shi et al.[7]

Hydrogen abstraction from CD_3CH_2Cl was also examined, using diode laser absorption, and found to have a rate constant of $k_1(CD_3CH_2Cl) = (6.0 \pm 1.0) \times 10^{-12}$ cm^3 s^{-1}. The ratio $k_1(CD_3CH_2Cl)/k_1(C_2H_5Cl) = 0.8 \pm 0.13$ agrees with that of the relative rate experiments (0.86 ± 0.1) in ref 7.

(b) Secondary HCl Formation. To identify the radical precursor of the secondary HCl, experiments were performed both in the presence and absence of NO. Figure 4 presents diode laser data from the photolysis of a $Cl_2/C_2H_5Cl/O_2/N_2/NO$ gas mixture, whereas Figure 5, illustrates the [HCl] time dependence for the same mixture in the absence of NO. The ratio of secondary to primary HCl generated is comparable in each case although the

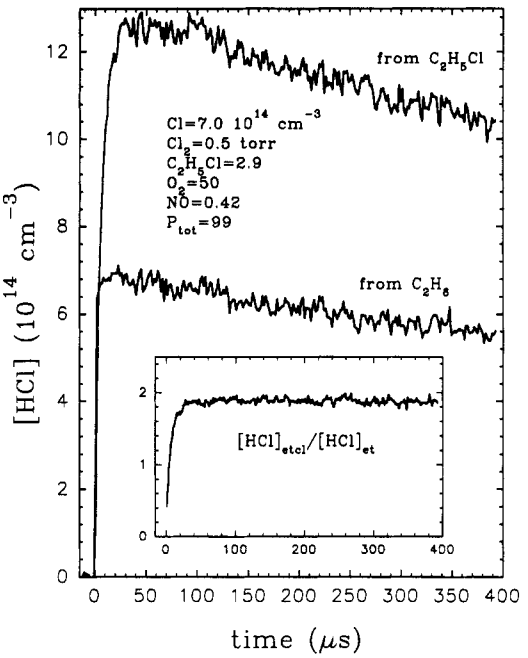

Figure 4. HCl concentration vs time following photolysis of a $Cl_2/C_2H_5Cl/O_2/N_2/NO$ gas mixture and the comparison when C_2H_5Cl is substituted by ethane. The inset shows the ratio of HCl produced from C_2H_5Cl to that from C_2H_6.

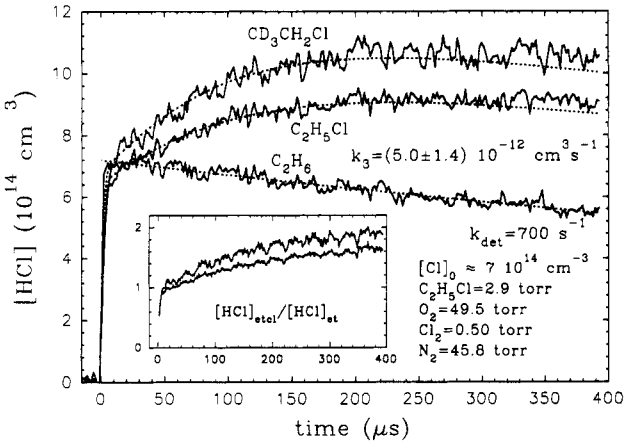

Figure 5. Comparison of the HCl concentration vs time for C_2H_5Cl, CD_3CH_2Cl, and C_2H_6. The ethane experiment illustrates the detector response, which shows an effective decay rate of 700 s^{-1} following the application of Beer's law. The ratios $[HCl]_{etcl}/[HCl]_{et}$ and $[HCl]_{dtcl}/[HCl]_{et}$ are shown in the inset and approach 1.8 and 2.0, respectively, at long times. The dotted lines represent the best fit, with respect to k_3, of the reaction model. (For the ethane trace, the fit is to an exponential decay.) The experimental conditions are those of experiments c and e. The small differences in primary HCl rise originate from variations in the chlorine flow and are accounted for in the analysis. The error in k_3 is the fitting error.

HCl in the absence of NO is still rising at the longest reaction time. In contrast, the rate of formation is approximately 30 times faster in the presence of NO. The data in Figure 6, which were obtained at a higher $[Cl]_0$, better illustrate that the secondary-to-primary HCl ratio in the absence of NO approaches the ratio observed in the presence of NO closely. The fact that the secondary to primary ratio is nearly identical both in the presence and absence of NO proves that the precursor species is the same for both mixtures. As discussed below, NO at 0.5 torr should react rapidly with CH_3CHClO_2 to form the alkoxy radical CH_3CHClO in this mixture. Thus, these time-resolved measurements of secondary HCl formation with and without NO provide strong evidence for the identification of the CH_3CHClO radical (see ref 7) as the source of the secondary HCl.

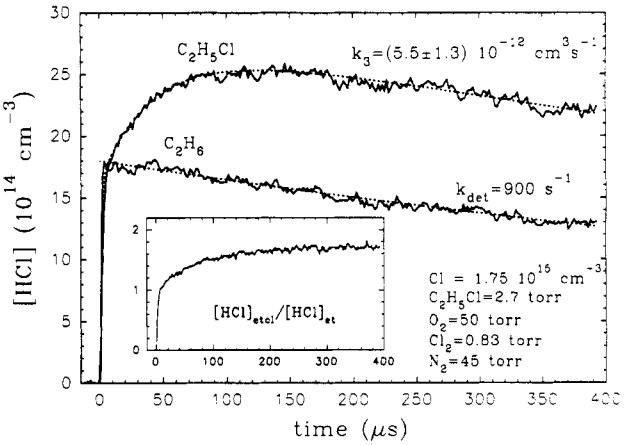

Figure 6. HCl concentration vs time as probed by diode laser absorption. The ethane experiment illustrates the detector response, which shows an effective decay rate of 900 s^{-1} following the application of Beer's law. The ratio $[HCl]_{etcl}/[HCl]_{et}$ is shown in the inset and approaches 1.75 at long times. The dotted lines represent the best fit, with respect to k_3, of the reaction model. (For the ethane trace, the fit is to an exponential decay). The experimental conditions correspond to experiment a. The error in k_3 is the fitting error.

The experiments with NO provide two additional pieces of information: estimates of the branching ratio of reaction 1 and an upper limit to the lifetime of CH_3CHClO. In the presence of NO, the alkoxy radical is formed by

$$CH_3CHClO_2 + NO \rightarrow CH_3CHClO + NO_2$$

Assuming a typical RO_2 + NO reaction rate constant of 1×10^{-11} cm^3 s^{-1} and [NO] = 1.4×10^{16} cm^{-3} yields a half-life of 5 μs for the alkoxy radical formation, which is entirely consistent with the data of Figure 4. The ratio of HCl formed from C_2H_5Cl versus that from C_2H_6 (inset of Figure 4) is 1.84 ± 0.1, indicating 84 ± 10% secondary HCl from the alkoxy radicals in the system. This value is less than 100% because, of the two sites available for hydrogen atom abstraction from ethyl chloride, only attack at the 1 position (reaction 1a) leads to CH_3CHClO and thence to secondary HCl. The observed 84% yield indicates that 84 ± 10% of the Cl atom reactions proceed via reaction 1a. This is consistent with the more accurate relative rate determinations[7,30] of $k_{1a}/(k_{1a}+k_{1b})$ [=0.82 ± 0.015]. Finally, the rate of secondary HCl formation in Figure 4 places a lower limit of $k_6 > 5 \times 10^5$ s^{-1} for elimination of HCl from CH_3CHClO. Analogous TRISP experiments at higher NO concentration place the lower limit to k_6 at about 2×10^6 s^{-1}.

The time dependence and magnitude of the secondary HCl rise in the absence of NO can be used to obtain the rate constant for the peroxy radical self-reaction and an estimate of its branching ratio. The diode laser measurements were fit to the reaction model of Table I with k_3 and k_{3a}/k_3 treated as adjustable parameters and $k_4 = k_3$. The results are given in Table II, and examples of the fits of the [HCl] time dependence are shown in Figures 5 and 6. The branching ratio of reaction 3 is found to be $k_{3a}/k_3 = 0.95 \pm 0.05$. It is relatively insensitive to k_3 and to the details of the reaction model, assuming that the alkoxy radical is the sole product of $CH_3CHClO_2 + RO_2$ cross reactions. The reported errors in k_{3a}/k_3 are a statistical combination of an approximately 5–10% fitting error and a 10% error due to the uncertainty in $[Cl]_0$. Combining the branching ratios of reactions 1 and 3 implies that the HCl concentration should rise to (1.78 ± 0.05)$[Cl]_0$, which is consistent with the $[HCl]_{etcl}/[HCl]_{et}$ traces shown in the insets of Figures 5 and 6.

The average of the four experimental determinations, reported in Table II, yields a rate constant of $k_3 = (5.2 \pm 1.3) \times 10^{-12}$ cm^3 s^{-1} for the CH_3CHClO_2 self-reaction. The error bars for k_3 listed in the table are a statistical combination of a 15–30% fitting error and a 20% uncertainty in $[Cl]_0$. Besides signal noise and the

TABLE II: Diode Laser Measurements of Secondary HCl Formation

	conditions[a]		results		
expt	$[Cl]_0$[b]	$[C_2H_5Cl]$[c]	k_3[d]	k_{3a}/k_3	three-center/ four-center
a	17.5	2.7	5.5 ± 1.3	0.9 ± 0.08	
b	12.1	3.8	5.0 ± 1.4	1.0 ± 0.1	
c	6.6	2.9	5.0 ± 1.4	1.0 ± 0.1	
d	5.0	3.8	5.0 ± 1.8	0.9 ± 0.15	
		av	5.2 ± 0.74	0.95 ± 0.05	
e	7.0	2.9 (CD_3CH_3Cl)	5.0 ± 2	1.0 ± 0.1	0.85–1.0

[a] $[Cl_2]$ = 0.5–0.8 Torr, $[O_2]$ = 50 Torr, and P_{tot} = 100 Torr; these remained approximately constant for all experiments. [b] Units are 10^{14} cm^{-3}. [c] Units are Torr. [d] Units are 10^{-12} cm^3 s^{-1}. Error bars include fitting error and the uncertainty in $[Cl]_0$, both of which are random from one experiment to another.

uncertainty in $[Cl]_0$, the fitting value for k_3 is also affected by the uncertainty in k_{3a}/k_3 and to the value of k_8 used for the reaction between CH_3CHClO_2 and the acetylperoxy radical. Tests indicate that doubling (halving) k_8 requires adjusting k_3 by ±1 × 10^{-12} cm^3 s^{-1} to reestablish a good fit. Doubling (halving) k_{12} or k_{17}, in contrast, has an insignificant effect on the secondary HCl formation. Thus, the experimental error of ±0.74 for the average value of k_3 is statistically combined with a 20% error due to uncertainties in the model and a 10% error due to k_{3a}/k_3 to yield the final error limits of ±1.3 × 10^{-12} cm^3 s^{-1} for k_3. The measured rate constant of k_3 = (5.2 ± 1.3) × 10^{-12} cm^3 s^{-1} is consistent with the self-reaction rate constants of other halogenated peroxy radicals,[4,24,31] in particular with the value of (6.0 ± 0.8) × 10^{-12} cm^3 s^{-1} we have measured for $CH_2ClCH_2O_2$.

Experiments were also performed using the TRISP apparatus to obtain the ratio of the total HCl generated to the primary HCl. These experiments were carried out at initial chlorine atom concentrations from 2 to 10 × 10^{15} cm^{-3} (obtained by varying $[Cl_2]_0$ or laser power) and at a very high C_2H_5Cl concentration (3 × 10^{17} cm^{-3}). Again, the results are complementary to the lower concentration data from the diode laser. Because the ethyl chloride concentration is very high, the primary HCl generation will occur very quickly and will be essentially complete after 2 μs. The secondary generation is observed to be complete after 100 μs in these experiments. Thus, a plot of the HCl concentration after 100-μs delay as a function of that obtained after 2 μs for different initial Cl atom concentrations will have as its slope the ratio of the total to the primary HCl yield. Such a plot is presented in Figure 7 yielding a slope of 1.71 ± 0.1. This is consistent with the ratio (=1.78 ± 0.05) derived from the diode laser experiments, providing additional verification of the magnitude of the time-resolved secondary HCl generation. Experiments were also performed using $[Cl_2]$ = 19 Torr, air = 730 Torr, but substituting C_2H_6 = 5 Torr for the C_2H_5Cl. In this experiment, the HCl rose rapidly at times less than 1 μs as presented in ref 14. The HCl concentration then remained constant to within ±5% for times from 1 to 100 μs. This verifies that the observed secondary rise in HCl when using C_2H_5Cl is not an artifact of the TRISP experiment.

The diode laser measurements of this ratio are more reliable because they provide an entire time profile rather than two data points per experimental condition. They are also less susceptible to uncertainty in this ratio caused by reaction 21, which is estimated to be ≤10% based on model calculations for the TRISP experiments. The TRISP data combined with the diode laser data show that, within experimental error, the ratio of the secondary to the primary HCl is independent of $[Cl]_0$ and C_2H_5Cl over factors of 20 and 4, respectively.

In Figure 1, the secondary HCl generation from the TRISP experiment is compared to the prediction of the extended model in Table I. To obtain this comparison, the primary HCl generation at times <5 μs was fitted to obtain the $[Cl]_0$ and k_1 appropriate

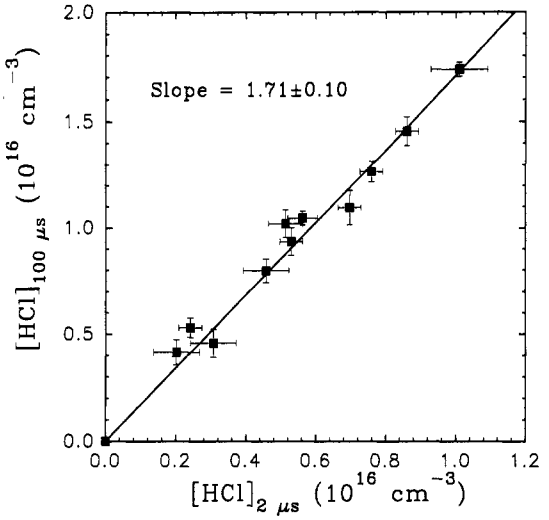

Figure 7. [HCl] (at 100 μs) plotted as a function of [HCl] (at 2 μs). Slope (=1.71 ± 0.1) represents the ratio of total HCl to primary HCl. C_2H_5Cl = 10 Torr, air = 715–735 Torr, Cl_2 = 14–35 Torr, laser power = 120–250 mJ.

to this data set as described in section IIIa. The model was then used to predict the secondary HCl formation. This model calculation is represented by the solid line in Figure 1. The fit, obtained without adjusting any other rate constants, is excellent, falling approximately 2% below the best line that could be drawn through the data at times >2 μs. The secondary HCl generation is sensitive to the presence of reaction 22 in these experiments, because it provides a path for release of the Cl that is stored as ClO by reaction 21. If ClO were a permanent sink for Cl (i.e., k_{22} = 0), the predicted total-to-primary HCl ratio would fall ≈12% below the experimental data. However, if k_{22} is reduced by a factor of 2, the predicted ratio falls by only 3%. Thus, the sensitivity to the value chosen for k_{22} is not great.

The agreement between the TRISP data and the model prediction provides strong confirmation that the secondary HCl is generated by radical–radical reactions. The model correctly predicts the observed large decrease in half-life for secondary HCl formation as $(Cl)_0$ increases by a factor of 15. For example, the experimental half-life for the secondary HCl generation decreases from 110 μs (see inset of Figure 5) to approximately 10 μs (see Figure 1) as the initial Cl atom density increases from 0.7 to 8.1 × 10^{15} cm^{-3}. This near inverse dependence of the half-life for secondary HCl generation on $[Cl]_0$ verifies that it forms as a result of a radical–radical reaction.

The data in ref 7 could only be interpreted in terms of a molecular elimination of HCl from a radical precursor and this interpretation is inherent in reaction 6 of our model. Because of the unusual nature of this elimination reaction, it is important to verify this assumption using the time-resolved data, if possible. In these time-resolved experiments, two other reactions could occur in which either Cl or H atoms are eliminated from the 1-chloroethoxy radical leading to excess HCl production:

$$CH_3CHClO \rightarrow CH_3CHO + Cl \quad (25)$$

$$\rightarrow CH_3COCl + H \quad (26)$$

The H atoms would then react according to

$$H + O_2 + M \rightarrow HO_2 + M \quad (k_{27} = 5.9 \times 10^{-32}\ cm^6\ s^{-1})^{22} \quad (27)$$

$$H + Cl_2 \rightarrow HCl + Cl \quad (k_{28} = 2 \times 10^{-12}\ cm^3\ s^{-1})^{32} \quad (28)$$

Both of these atom elimination reactions would, therefore, lead to chain propagation. Reactions similar to (25) have been

observed at room temperature for fully chlorinated alkoxy radicals (e.g., CCl_3O[22] and CH_3CCl_2O[33]). When either reaction 25 or 26 [with the addition of (27) and (28)] was substituted for reaction 6 in the mechanism, using the same rate constant as k_6, the dashed or dotted curves, respectively, in Figure 1 were obtained. Although the initial fit through 5 μs is very similar to that of the solid line, substitution of reaction 25 or 26 leads to a much greater secondary HCl generation because of the chain propagation. Between 5 and 50 μs, the experimental HCl data rise only 38% while substitution of reaction 25 or 26 results in increases of 90 and 115% in the predictions, respectively. Thus, the time-dependent data in Figure 1 (and also Figures 5 and 6) support the molecular elimination mechanism proposed in ref 7. Furthermore, as shown in Figure 4, the HCl concentration in the presence of NO rises rapidly to a value of $1.84[Cl]_0$ and subsequently remains constant for times longer than 20 μs, showing no indication of chain propagation.

(c) Secondary HCl from CD_3CH_2Cl. The time-resolved data confirm elimination from CH_3CHClO as the source of secondary HCl, as was inferred from the FTIR product study.[7] However, this additional HCl could arise from either three- or four-center elimination (i.e., the H and Cl atoms come from the same or different C atoms in the radical, respectively). To explore the elimination mechanism, experiments were performed using CD_3CH_2Cl. If the alkoxy radical decomposition proceeds by four-center elimination, DCl should be formed and a reduction in the secondary HCl yield would be observed.

Figure 5 compares diode laser measurements of the HCl generated from the Cl-initiated oxidation of CD_3CH_2Cl to that from C_2H_5Cl under essentially the same experimental conditions. Note in Figure 5 that the initial Cl atom concentration for the C_2H_5Cl experiment is approximately 5% less than for the C_2H_6 or CD_3CH_2Cl. After correction for this difference, more rather than less secondary HCl is generated from the deuterated compound. The explanation is that the branching ratio for reaction 1 changes upon deuteration, with 97% of the reaction proceeding via hydrogen abstraction from the 1 position.[7] Thus the expected yield of CD_3CHClO_2 is 15% larger than for the protonated compound and the observed 12% increase implies that little DCl is formed from the CD_3CHClO radical. A fit of the data to the reaction model of Table I is shown in Figure 5. Inserting the values $k_3 = 5.0 \times 10^{-12}$ cm^3 s^{-1} and $k_{3a}/k_3 = 0.95$, determined from the accompanying experiment with C_2H_5Cl, into the model in Table I and fitting the model to the data yields a ratio of 0.85–1.0 for the branching ratio three-center/four-center elimination.

IV. UV Measurements

(a) UV Absorption Spectra. Absolute UV absorption cross sections for CH_3CHClO_2 and $CH_2ClCH_2O_2$ are displayed in Figure 8. They were determined by measuring their absorbance relative to that of ethylperoxy radicals and scaled using the known UV cross section[18] for $C_2H_5O_2$. The chloroethylperoxy radicals (9×10^{14} cm^{-3}) were generated by photolysis of $Cl_2/C_2H_5Cl/O_2/N_2$ and $Cl_2/C_2H_4/O_2/N_2$ gas mixtures, respectively. $CH_2ClCH_2O_2$ is formed with the absence of CH_3CHClO_2 via

$$Cl + C_2H_4 + M \rightarrow CH_2ClCH_2 + M$$

$$CH_2ClCH_2 + O_2 + M \rightarrow CH_2ClCH_2O_2 + M$$

The absorbance was measured at 20 μs following the photolysis pulse. The C_2H_4 and O_2 concentrations were varied to ensure that both of these reactions went to completion, and the absorption intensity was corrected for the ≈5% loss of $CH_2ClCH_2O_2$ radicals by self-reaction in the time between photolysis and absorption measurement. The error is estimated at ±10%, with 5% originating from uncertainty in $\sigma(C_2H_5O_2)$ and the remainder

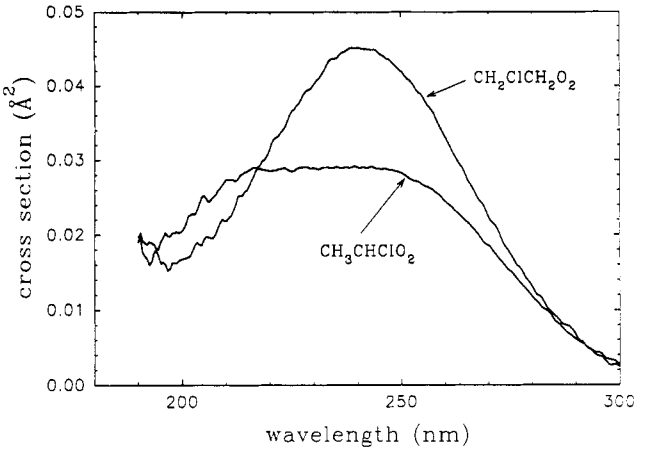

Figure 8. UV absorption cross section vs wavelength for CH_3CHClO_2 and $CH_2ClCH_2O_2$. The estimated error is ±10%.

due to possible variations in experimental conditions between the $CH_2ClCH_2O_2$ and $C_2H_5O_2$ measurements.

Photolysis of Cl_2 in the presence of C_2H_5Cl and O_2 results in a mixture of 82% CH_3CHClO_2 and 18% $CH_2ClCH_2O_2$. As above, the absorbance of this mixture relative to that of $C_2H_5O_2$ generated under the same conditions was scaled by the ethylperoxy cross section. The CH_3CHClO_2 cross section was then determined by subtracting the $CH_2ClCH_2O_2$ component and scaling the remainder to 100%.

The (2-chloroethyl)peroxy UV spectrum is very typical of alkylperoxy radicals. In fact, with $\sigma_{max} = 0.045$ Å^2 at 240 nm, it is nearly indistinguishable from the spectrum of $C_2H_5O_2$, for which $\sigma_{max} = 0.046$ Å^2 at 239 nm. The shape and position of σ_{max} are in excellent agreement with the previous measurement of Dagaut et al.,[34] but the cross sections are about 13% larger. The spectrum of CH_3CHClO_2, in contrast, is quite different, exhibiting a low, broad absorption maximum of 0.029 Å^2 over the 215–248-nm range. While this is not typical of peroxy UV spectra, $CF_3CCl_2O_2$ also exhibits similar features.[35]

(b) Kinetics. $CH_2ClCH_2O_2$ radicals formed following the photolysis of a $Cl_2/C_2H_4/O_2/N_2$ mixture are expected to decay via self-reaction to form the corresponding alkoxy radicals. In analogy with other alkoxy species, these can react with O_2, reaction 16, to form HO_2 which can then react with the parent peroxy radical, further contributing to its decay. Therefore, the time-resolved UV spectra recorded following the photolysis pulse were fit to a linear combination of the $CH_2ClCH_2O_2$ and HO_2 reference spectra and to the residual UV absorbance found 40 ms after the laser pulse. The last component was included to take into account a small (<10%) contribution from stable UV absorbing reaction products.

The best fit $CH_2ClCH_2O_2$ and HO_2 concentration versus time profiles determined by the fitting procedure are illustrated in Figure 9. The $CH_2ClCH_2O_2$ concentration decays with an observed second-order rate constant of $(6.0 \pm 0.8) \times 10^{-12}$ cm^3 s^{-1}. The error (95% confidence) is a combination of a 7% fitting error, a 10% error in UV cross section, and a 7% error which accounts for the effect on the $CH_2ClCH_2O_2$ concentrations if HO_2 or the residual absorbance are omitted from the fitting procedure. The present value of $k_{5_{obs}}$ is 67% larger than reported previously by Dagaut et al.[34] While a small (~12%) part of this can be attributed to the larger $CH_2ClCH_2O_2$ UV cross section obtained in the present work, a 53% discrepancy remains. Typically, the observed second-order peroxy radical decay rate is corrected for secondary reaction with HO_2.[24] In the present case, however, such a correction would be inconsistent with the small level of HO_2 observed. A model based on reactions 5, 16, and 20, assuming a rate constant of 7×10^{-12} cm^3 s^{-1} for the $CH_2ClCH_2O_2 + HO_2$ reaction, leads a peak concentration of

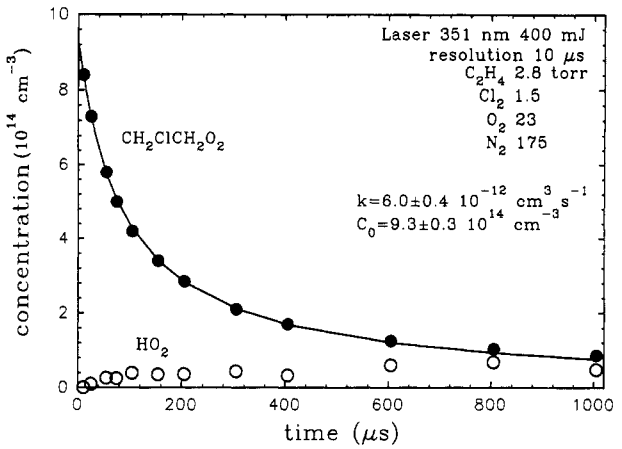

Figure 9. $CH_2ClCH_2O_2$ concentration versus time. Concentrations were determined from a two parameter fit of the time resolved absorbances to the $CH_2ClCH_2O_2$ reference spectrum and the residual spectrum. The solid line shows the fit to a second-order rate law.

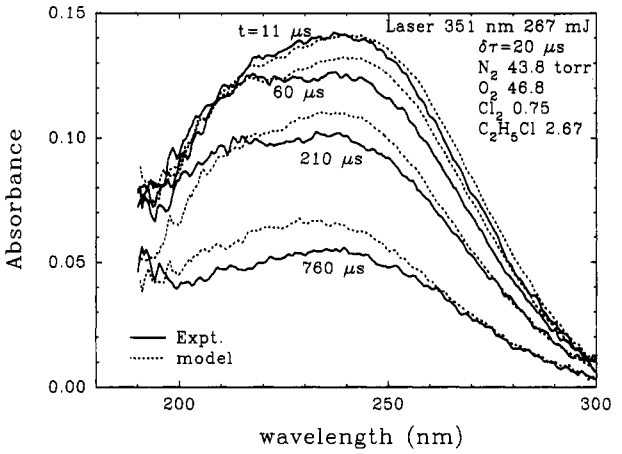

Figure 10. Time-resolved UV absorption spectra following photolysis of a $Cl_2/C_2H_5Cl/O_2/N_2$ gas mixture. The dashed lines show the absorbance which is calculated from the CH_3CHClO_2, $CH_2ClCH_2O_2$, $CH_3C(O)O_2$, CH_3O_2, and HO_2 concentrations predicted by the model and the reference UV cross sections and to which the appropriate fraction of the residual (40 ms) absorbance has been added. δt is the time resolution.

$[HO_2]_{max} = 2.4 \times 10^{14}$ cm^{-3}, considerably higher than is observed. The predicted peak HO_2 concentration can be lowered by increasing the rate constant to 4×10^{-11} cm^3 s^{-1}; however, then the predicted $CH_2ClCH_2O_2$ concentration profile deviates significantly from second order. More likely, reaction 16 proceeds with a rate constant of $k_{16} < 1 \times 10^{-15}$ cm^3 s^{-1}, in which case secondary consumption of $CH_2ClCH_2O_2$ by HO_2 becomes insignificant.

Time-resolved UV spectra following photolysis of a $Cl_2/C_2H_5Cl/O_2/N_2$ gas mixture are shown in Figure 10. A simple second-order decay of CH_3CHClO_2 is not indicated. If a rate constant were estimated from the decrease in absorbance at 240 nm ($t_{1/2} \approx 300$ μs and $[CH_3CHClO_2]_0 = 9.3 \times 10^{14}$ cm^{-3}) the result, 2×10^{-12} cm^3 s^{-1}, would be considerably smaller than the value obtained above from the rise in secondary HCl. Furthermore, the spectra become broader and shift to shorter wavelength as time progresses. There are a number of reasons for this which become apparent upon consideration of the reaction model in Table I and the discussion in ref 7. At early times there is a 0.82/0.18 mixture of the 1- and (2-chloroethyl)peroxy radicals. From the above IR and UV measurements, these self-react with approximately the same rate constant. However, whereas the $CH_2ClCH_2O_2$ self-reaction eventually leads to HO_2 as a secondary absorbing species, the CH_3CHClO_2 self-reaction leads, after HCl elimination from the alkoxy radical, to CH_3CO. This species rapidly adds O_2 to form $CH_3C(O)O_2$ which has a strong UV

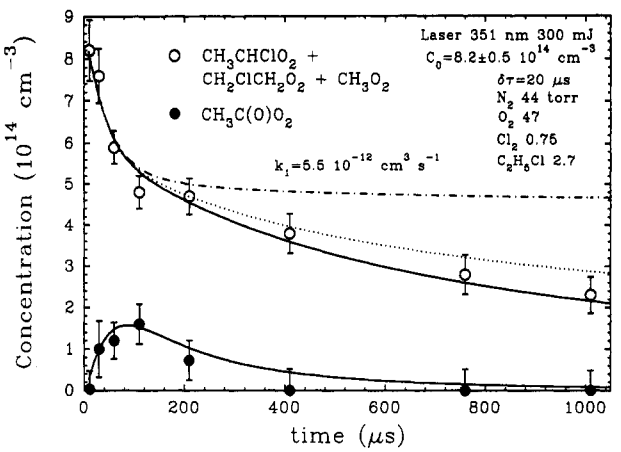

Figure 11. Comparison of experimental vs model predictions of the $CH_3CHClO_2 + CH_2ClCH_2O_2 + CH_3O_2$ and $CH_3C(O)O_2$ concentrations. The error bars are 95% confidence intervals for the fit of the time resolved absorbances, which were doubled to account for uncertainties in the model. The dotted line is obtained by setting the rate constants for the HO_2 reactions to zero (k_{17}, k_{18}, k_{19}, and k_{20}). The dot–dash line shows the predictions when the rate constants for reactions 13 and 14 are also set to zero.

absorption band[24] peaking at about 210 nm. Furthermore, self-reaction of the aetylperoxy radical (or reaction with other peroxy species) produces CH_3CO_2, which rapidly dissociates to form CH_3.[21,23] The methyl radical adds O_2 to form CH_3O_2 which has $\sigma_{max} = 0.041$ Å^2 at 238 nm.[18] Finally, the various alkoxy radicals that are produced in the course of these reactions form HO_2 upon reaction with O_2, which has $\sigma_{max} = 0.040$ Å^2 at 208 nm.[24] Thus, the shift in time of the absorbance to shorter wavelengths arises from the formation of $CH_3C(O)O_2$ and HO_2. The slower than expected decrease in the absorbance at 240 nm is due to the fact that CH_3CHClO_2 lost by self-reaction is, at least partially, replaced by CH_3O_2.

Because of the large number of peroxy radicals with overlapping UV absorption spectra, the time resolved spectra shown in Figure 10 could not be decomposed into all of their constituents. Instead, two methods were employed to compare predictions from the reaction model to the experimental measurements. The first was to use the peroxy radical concentrations predicted by the model in conjunction with the reference UV absorption spectra to construct the composite UV absorbance at a time t after initiation of the reaction by the photolysis pulse. For this purpose, the value of k_3 obtained from fitting the secondary HCl rise was used. Comparisons to the experimental absorbances are shown by the dashed lines in Figure 10. The predictions mimic semiquantitatively the observed UV absorbances; the absorption maximum decreases with time and shifts to the blue, and a shoulder develops at 210 nm and subsequently disappears. As expected, the predictions become poorer at longer times due to the proliferation of secondary peroxy radical reactions with uncertain or unknown reaction rate constants.

In the second method, the time-resolved UV absorbances were fit, using four adjustable parameters, to the following reference spectra: a linear combination of $(0.82\sigma(CH_3CHClO_2) + 0.18\sigma(CH_2ClCH_2O_2))$, $\sigma(CH_3C(O)O_2)$, $\sigma(HO_2)$, and the absorbance spectrum 40 ms after the photolysis pulse. Actually, the composite (chloroethyl)peroxy spectrum is sufficiently similar to the spectrum of CH_3O_2 that this component of the total absorbance will include also the methylperoxy radical concentration, i.e., it will approximately yield $[CH_3CHClO_2] + [CH_2ClCH_2O_2] + [CH_3O_2]$. The approximation should be good at early times, when relatively little CH_3O_2 is expected, but will degrade as time progresses. The 40-ms spectrum is included in the fit to account for various stable UV absorbing species produced during the course of the reaction. Figure 11 compares this experimental estimate of the $(CH_3CHClO_2 + CH_2ClCH_2O_2 +$

CH_3O_2) and $CH_3C(O)O_2$ concentrations that are obtained from the spectral fitting procedure to the prediction from the reaction model of Table I (solid line). The model prediction is based on the rate constant of $k_3 = 5.2 \times 10^{-12}$ cm^3 s^{-1} obtained from the transient HCl formation experiments. It gives a good fit to the data, which may be fortuitous given the approximations discussed above.

V. Conclusion

The IR and UV spectroscopic studies described in this paper follow the Cl initiated oxidation of ethyl chloride in real time. The IR measurements show an unexpected two stage formation of HCl, in which the stages have very different half-lives. The primary HCl is formed rapidly from the attack of C_2H_5Cl by chlorine atoms, with a rate constant of $(7.3 \pm 0.9) \times 10^{-12}$ cm^3 s^{-1}. The ratio of total HCl generated at long times to the primary HCl is observed to be 1.78 ± 0.1. In the absence of NO, the precursor of the secondary HCl is formed by a radical–radical process, as demonstrated by the nearly inverse dependence of the rise time of secondary HCl on the initial Cl-atom concentration. Fits to the experimental data using the mechanism in Table I determine that the reaction rate constant for the CH_3CHClO_2 self reaction is $k_3 = (5.2 \pm 1.3) \times 10^{-12}$ cm^3 s^{-1}. When 0.4 Torr of NO is added, the rate of secondary HCl generation increases by a factor of 30 to a level consistent with typical NO + peroxy radical rate constants. However, the amount of secondary HCl generated is the same to within 5% both in the presence and absence of NO, providing strong evidence that the secondary HCl forms via elimination from the CH_3CHClO radical intermediate. Substituting CD_3CH_2Cl for C_2H_5Cl produces a 12% *increase* in the secondary HCl yield. This can be explained by the mechanism in Table I and shows that 85–100% of the secondary HCl originates from three-center elimination.

The UV data show a rapid formation of (chloroethyl)peroxy radicals, as expected in the presence of excess O_2, followed by a decay of the radicals which is consistent with the self reaction rate constant of $(5.2 \pm 1.3) \times 10^{-12}$ cm^3 s^{-1} determined in the IR experiments. The decay, however, does not proceed via a simple loss of the chloroethylperoxy radicals. Instead, the spectra shift to the blue with increasing time, indicating the birth and subsequent decay of another radical, which we identify with $CH_3C(O)O_2$. The CH_3CO fragment that remains after HCl elimination from CH_3CHClO rapidly adds O_2 and along with formation of HO_2 is responsible for the blue shift observed in the time-resolved UV spectra.

HCl elimination from CH_3CHClO represents a new reaction pathway for alkoxy radicals. It is possible that similar elimination channels exist for other halogenated alkoxy species. If this turns out to be the case, then this elimination mechanism may be important to understanding atmospheric oxidation chemistry.

References and Notes

(1) Atkinson, R. *J. Phys. Chem. Ref. Data* **1989**, Monograph No. 1.
(2) Atkinson, R. *Atmos. Environ.* **1990**, *24A*, 1.
(3) Wallington, T. J.; Hurley, M. D.; Ball, J. C.; Kaiser, E. W. *Environ. Sci. Technol.* **1992**, *26*, 1318.
(4) Maricq, M. M.; Szente, J. J. *J. Phys. Chem.* **1992**, *96*, 10862.
(5) Nielsen, O.-J.; Ellermann, T.; Sehested, J.; Wallington, T. J. *J. Phys. Chem.* **1992**, *96*, 10875.
(6) Sehested, J.; Ellerman, T.; Nielsen, O.-J.; Wallington, T. J.; Hurley, M. D. *Int. J. Chem. Kinet.*, in press.
(7) Shi, J.; Wallington, T. J.; Kaiser, E. W. *J. Phys. Chem.* **1993**, *97*, 6184.
(8) Seakins, P. W.; Leone, S. R. XXth Informal Conference on Photochemistry, April 1992.
(9) Seakins, P. W.; Woodbridge, E. L.; Leone, S. R. *J. Phys. Chem.* **1993**, *97*, 5663.
(10) Arunan, E.; Wategoankar, S. J.; Setser, D. W. *J. Phys. Chem.* **1991**, *95*, 1539.
(11) Tsai, C.-P.; McFadden, D. L. *J. Phys. Chem.* **1989**, *93*, 2471.
(12) Maricq, M. M.; Szente, J. J.; Kaiser, E. W. *J. Phys. Chem.* **1993**, *97*, 7970.
(13) DeMore, W. B.; Sander, S. P.; Golden, D. M.; Hampson, R. F.; Kurylo, M. J.; Howard, C. J.; Ravishankara, A. R.; Kolb, C. E.; Molina, M. J. Chemical Kinetics and Photochemical Data for Use in Stratospheric Modeling, JPL publication 92–20, 1992.
(14) Kaiser, E. W.; Rimai, L.; Schwab, E.; Lim, E. C. *J. Phys. Chem.* **1992**, *96*, 303.
(15) Rimai, L.; Kaiser, E. W.; Schwab, E.; Lim, E. C. *Appl. Opt.* **1992**, *31*, 350.
(16) Tschuikow-Roux, E.; Salomon, D. R. *J. Phys. Chem.* **1987**, *91*, 699.
(17) Leone, S. R. *J. Phys. Chem. Ref. Data* **1982**, *11*, 953.
(18) Maricq, M. M.; Wallington, T. J. *J. Phys. Chem.* **1992**, *96*, 986.
(19) Atkinson, R.; Baulch, D. L.; Cox, R. A.; Hampson, R. F.; Kerr, J. A.; Troe, J. *J. Phys. Chem. Ref. Data* **1992**, *21*, 1125.
(20) Westley, J. T.; Herron, J. T.; Cvetanovic, R. J.; Hampson, R. F.; Mallard, W. G. NIST Chemical Kinetics Data Base, NIST, Gaithersburg, MD, 1991.
(21) Moortgat, G. K.; Veyret, B.; Lesclaux, R. *J. Phys. Chem.* **1989**, *93*, 2362.
(22) Atkinson, R.; Baulch, D. L.; Cox, R. A.; Hampson, R. F., Jr.; Kerr, J. A.; Troe, J. *J. Phys. Chem. Ref. Data* **1989**, *18*, 881.
(23) Horie, O.; Moortgat, G. K. *J. Chem. Soc., Faraday Trans.* **1992**, *88*, 3305.
(24) Wallington, T. J.; Dagaut, P.; Kurylo, M. J. *Chem. Rev.* **1992**, *92*, 667.
(25) Maricq, M. M.; Szente, J. J.; Shi, J.; Kaiser, E. W., unpublished data.
(26) Baer, S.; Hippler, H.; Rahn, R.; Siefke, M.; Seitzinger, N.; Troe, J. *J. Phys. Chem.* **1991**, *95*, 6463.
(27) Dagaut, P.; Wallington, T. J.; Kurylo, M. J. *J. Photochem. Photobiol. A: Chem.* **1989**, *48*, 187.
(28) Simon, F. G.; Burrows, J. P.; Schneider, W.; Crutzen, P. J. *J. Phys. Chem.* **1989**, *93*, 7807.
(29) Wine, P. H.; Semmes, D. H. *J. Phys. Chem.* **1983**, *87*, 3572.
(30) Niedzielski, J.; Tschuikow-Roux, E.; Yano, T. *Int. J. Chem. Kinet.* **1984**, *16*, 621.
(31) Maricq, M. M.; Szente, J. J. *J. Phys. Chem.* **1992**, *96*, 4925.
(32) Baulch, D. L.; Duxbury, J.; Grant, S. J.; Montague, D. C. *J. Phys. Chem. Ref. Data* **1981**, *10*, Suppl. 1, 1.
(33) Nelson, L.; Shanahan, I.; Sidebottom, H. W.; Treacy, J.; Nielsen, O. J.; *Int. J. Chem. Kinet.* **1990**, *22*, 577.
(34) Dagaut, P.; Wallington, T. J.; Kurylo, M. J. *Chem. Phys. Lett.* **1988**, *146*, 589.
(35) Jemi-Alade, A. A.; Lightfoot, P. D.; Lesclaux, R. *Chem. Phys. Lett* **1991**, *179*, 119.